Article

Maintenance Cycle Reduction Time and Energy Savings of Mechanical Face Seals Using Thermodynamic FEM Analysis

Andrei Zoltan Farkas [1], Veronica Argeșanu [1], Beniamin Boșcai [2,*] and Denisa Abrudan [2]

1   Mechatronics Department, Mechanical Faculty, Timișoara Polytechnic University, 2 Piața Victoriei, 300006 Timisoara, Romania
2   Management Department, Faculty of Economics and Business Administration, West University Timișoara, 16 Johann Heinrich Pestalozzi Street, 300115 Timisoara, Romania
*   Correspondence: beniamin.boscai@e-uvt.ro; Tel.: +40-784-220-916

Abstract: The lifetime cost evaluation of a seal must take into account all expenses throughout its operation. The thermodynamic aspects of mechanical face seals (MFSs) analyzed using FEM for various pairs of materials and their correlation with wear, reliability, and economic feasibility have not been researched in the literature. The MFSs analyzed in this paper were manufactured by ROSEAL S.A. for use in water pumps. The materials of the primary seal rings used by manufacturers were taken into account. The operating conditions were as follows: n = 3000 rpm, water temperature = 80 °C, and pressure = 0.1 MPa. In our study, we focused on the thermodynamic phenomena occurring in the MFS. The thermodynamic simulation was run using the FEM software MSC Nastran. Maps of the temperatures and the heat flow in the primary seal rings, for the two types of MFS and for different pairs of materials, were obtained using FEM analysis. The results highlight that the flow rate of leaks increases linearly with the angular speed of the pressure ring and is independent of the materials used in the primary seal.

Keywords: mechanical face seals; thermodynamical FEM analysis; energy saving; reliable design

1. Introduction

The evaluation of the lifetime cost of a seal, which, in theory, is extremely long [1], must take into account not only the initial cost of acquisition, but also all expenses that occur throughout its operation [2] (operating costs, replacement of parts, power consumption, fluid losses, cost of stocking spare parts, production losses, auxiliary aggregates, secondary defects, product contamination, and environmental pollution).

Identifying the pairs of materials from which the two main sealing components are made may have a positive impact on optimizing energy–economy–environment systems and ultimately contribute to global energy efficiency.

In particular, this happens by increasing the life expectancy of the seals, which automatically generates lower operating costs, reduces maintenance costs, reduces losses from equipment downtime during repair, avoids the risk of other equipment failures, and directly contributes to the reduction in CO_2.

This research is related to the water industry in Romania, particularly to drinking water and sewage pumping systems. These systems, in addition to the initial costs of production, assembly, commissioning, and energy consumption for their operation, have annual expenses generated by maintenance. An important component of maintenance activity includes the replacement of mechanical seals, considered as wear parts.

According to a previous report, the market size of mechanical seals was valued at 3.64 billion EUR in 2022 [3].

The costs of replacing the mechanical seals of the pumps and returning them to original operating conditions are summarized in Table 1. We took into account the preventive maintenance only (which represents considerable costs every year).

Table 1. Maintenance costs simulation.

No.	Motor Power [kW]	Labor [h]	Labor Costs [EUR/h]	Labor Value [EUR]	Seal Value [EUR]	Cost per kW [EUR]	Cost per kW/h [EUR]	Lost Energy per hour [EUR/h]
1	11.5	24	20	480	1951	0.77	8.80	0.05
2	44	48	20	960	2565	0.77	33.68	1.71
3	44	48	20	960	2565	0.77	33.68	1.71
4	65	52	20	1040	3651	0.77	49.76	1.71
5	65	52	20	1040	3651	0.77	49.76	1.71
6	4.5	16	20	320	1675	0.77	3.44	0.57
7	2.5	12	20	240	921	0.77	1.91	0.57
Total	236.5	152	20	5040	16,979	0.77	181.05	8.06

Other costs that are essential for such an intervention were not included (bearings, painting, resistant abrasive solutions, other axle repairs, transport, etc.). We narrowed our focus to only consider the sewage pumps of a municipal sewage treatment plant serving over 300,000 inhabitants made by only one in four or five pump manufacturers (which can be up and running at any given moment); there are an even greater number of products and pumps than those listed below within the treatment plant.

In Table 1, by adding all existing pumps at the city level, we can extrapolate that the derived costs and effects would be significantly larger.

SC Hidropump SRL, the local company in charge of the maintenance and repair of these pumps, provided initial data gathered from repair reports.

Table 1 shows the costs of preventive maintenance for a 1-year period. The costs for other manufacturers' pumps and other equipment with mechanical seals incorporated in their design were not subject of this analysis. This also applies to the cost related to industrial consumption (which is massive in terms of equipment seals and energy consumption), pumps from residential and commercial housing, municipal buildings, water supply stations, fire pumping stations, or the problems generated by nonoperational equipment.

The CO_2 emissions due to the production of these seals are another important factor not considered in the current analysis [4]. On a local level, the focus of public administrations on reducing CO_2 emissions can be seen in various projects on sustainable energy, such as the Action Plan for Sustainable Energy of the Municipality of Timișoara (Planul de Acțiune pentru Energia Durabilă a Municipiului Timişoara) [5].

This research can make strong contributions over time in cutting down maintenance expenses, as well as in terms of a social, economic, and environmental impact with respect to sustainable energy.

The performance of front seals can influence the overall energy efficiency. In the future, a thorough evaluation of each mentioned sector can make an important contribution to reducing energy consumption [3].

For small seals, 1–2 inches (25–50 mm) in diameter, we have a relatively low energy consumption of 1 hp (0.75 kW). However, larger seals can consume more than 3 hp (2.24 kW) of power [6].

Analyzing the data within the table, we can find a total energy loss of 8.6 EUR/h for the conditions stated above, while the loss in inefficient systems can be as much as 4%.

There are other types of rotary shaft seals; however, according to Table 2, mechanical face seals (MFSs) are clearly superior. A comparative analysis of MFSs and other rotary shaft seals based on technological, operating, and cost criteria is presented.

Table 2. Specification: parameters and functional conditions comparison between face seals and rotary shaft seals [7].

Specification: Parameters/Functional Conditions	Types of Seal	
	Face Seal	Rotary Shaft Seal
0	1	2
Materials and execution technology	pretentious, involves polishing the active surfaces of the rings	unpretentious, for the sealing edge E class of precision is needed
Mounting space	for d = idem maximum	minimum
The machining conditions of the shaft	advance correction	
	radial + axial	radial
The possibility of compensating the deviations of the shape and position of the shaft	very good	medium/good
Shaft wear	null	existing/significant
Power dissipation through friction	reduced	loaded: high / unloaded: reduced
Maintenance costs	reduced	
Living costs	comparable	
Initial costs	high	low
lubrication/cooling measures	required	
The nature of the fluid	no restrictions	limited depending on the compatibility with the material of the sleeve

In the literature [8–11], problems of frictional couplings are analyzed, respectively, of MFSs under various aspects.

From a functional point of view, MFSs are considered by researchers and engineers zero-leakage seals. While being used to seal fluids that vary from water to propane propylene or diesel [12], they are found to work successfully with both gas and liquids in extreme conditions such as those of aero-engines upstream pumps [13] or other volatile media such as hydrocarbon mixtures in petrochemical plants if the thermophysical properties of the sealed medium are well expressed [14]. Guidelines for estimating the wear of the MFS when functioning under friction instability conditions are found in the literature [15].

From an analytical point of view regarding the thermal behavior, the importance of the thermal conductance factors is found in the literature [16]; models for the heat fluxes between fluids and solids, enthalpy of the fluid, and the vapor mass fraction, using Newtons method [17] and mathematical analysis for non-contacting (gas lubricated) MFSs [18] develop more detailed mathematical models describing physical phenomena.

The tribological aspects of MFS are well explored in the literature, from the influence of the waviness of the rings to the viscosity–temperature effect in the main contact area of the MFS [19,20], the common tribological concerns of the influence of surface roughness on temperatures [21], and research on reducing temperatures in dry contact through surface texturing with graphite [22–24] to the potential use of superconducting magnetic force fields to improve carrying capacity and lubrication characteristics under heavy loading conditions [25].

Thermodynamic analyses carried out with the finite element method (FEM) on dry friction couplings of general mechanical seals [26] and general thermodynamic FEM simulations are found in the literature [27], but there is a lack of research on MFSs with lubricated interfaces.

From an experimental perspective, we found data about various pairs of materials tested for the friction and wear behavior, in dry sliding contact seals or lubricated [28,29].

In conclusion, the thermodynamic aspects of the MFS analyzed with FEM for various pairs of materials of the primary seal of the MFS, and the connection between them and the wear, reliability and economic implications in the operation fields of the equipment in which MFS are found, are not addressed in the literature.

Active control of the MFS will overcome the limitation of reliability, allowing a particularly reliable seal and a priori estimation of wear over time. Increasing the life of MFSs offers great economic benefits in top fields, such as nuclear, aeronautical, chemical, petrochemical, pharmaceutical, food, domestic, and transportation fields [30].

2. Fundamentals of Thermo-Hydrodynamics of an MFS in the Non-Isothermal Stationary Regime Analyzed by FEM

A realistic approach to the MFS phenomenology can only be made through a thermo-hydrodynamic (THD) or even thermo-elasto-hydrodynamic (TEHD) analysis [27].

The decisive consequences of optimizing the operation of an MFS resulting from finding the compromise between high durability and low leakage rates are as follows:

- A very small thickness of the fluid film that leads to the production of an appreciable amount of heat in the interface of the primary seal;
- The thermoelastic deformations of the rings, although reduced in absolute value, are comparable to the thickness of the film, significantly influencing the geometric configuration of the interface.

The main source of heat production in an MFS is friction from the interface (Figure 1). Heat removal from the seal is mainly achieved by the movement of the sealed fluid.
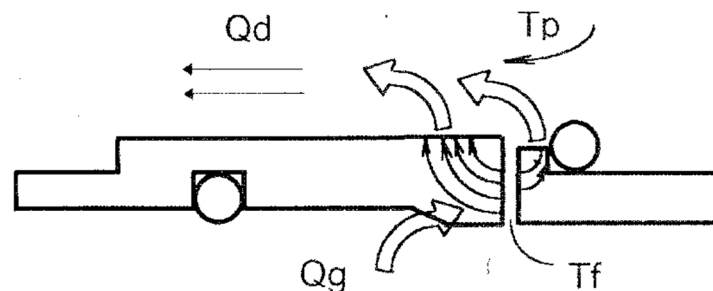
Figure 1. Temperature flows from the MFS interface [31], where Qd—dissipated heat; Qg—generated heat; Tf—temperature in the interface; Tp—temperature of the sealed fluid.

If the film in the interface is heated above the boiling point at the pressure in the film, then it will evaporate causing malfunction and eventually the seal is destroyed.

An elementary numerical analysis shows that the role of the leakage flow in cooling the interface is insignificant so that the entire amount of heat is practically taken over by the two rings of the primary seal.

In this context, an essential aspect of the heat transfer study is represented by the quantities produced in the interface between the pressure ring and the friction ring. If the temperature of the sealed fluid is known, the modeling of the temperature field can be restricted to the two rings with the consideration of convection with the fluid.

If the correlation of interface geometry with the thermal deformations of the rings (THD problem) is taken into account, then in the system of equations of MFS modeling with fluid film, the equations of thermo-elasticity, associated with the condition of resting the two rings, must be added.

Instabilities of any kind are the main cause of premature retirement of an MFS that theoretically works with fluid film [7]. The effect of temperature manifests itself on three levels, all of which significantly influence the operation of the MFS:

- By the phase change of the fluid in the interface (vaporization);
- On the opening force through the variation of fluid viscosity;
- On the elastic deformations of the rings.

All analytical THD models of fluid film MFSs resort to a simplification of the heat flux line trajectories in the pressure ring of the seal and neglect the heat conduction in the friction ring.

From this it follows that the thermal conductivity of the material of the friction ring would be unimportant.

Extending the use of FEM as an effective tool for analyzing the behavior of structures from a mechanical and thermal point of view has as a consequence the continuous enrichment of knowledge of the intimate phenomena that govern the behavior of MFS.

The MFS assembly indicates the same position for thermal and mechanical loading. Because of this, geometric symmetries will also be symmetries of thermal load.

When determining by calculation using FEM, there is the advantage of determining the temperature in a large number of internal points of the primary sealing rings, the results depending on the extent to which the contour conditions were adopted according to the actual operating conditions.

3. Theoretical Bases of the FEM in Two-Dimensional and Axially Symmetric Problems of Heat Transfer in the Stationary Regime

3.1. Two-Dimensional Problems

The steady-state heat exchange of a body with the environment, in the case of two-dimensional problems (Figure 2), is expressed by the equation:

$$\frac{\partial}{\partial x}\left(\lambda_x \frac{\partial \theta}{\partial x}\right) + \frac{\partial}{\partial x}\left(\lambda_y \frac{\partial \theta}{\partial x}\right) + M - q + \alpha(\theta - \theta_e) = 0 \tag{1}$$

Heat exchange by convection: $\alpha S_3(\theta - \theta_e)$ with the boundary conditions:

$$\theta = \theta(x, y), \text{ the temperature imposed on the surface } S_1;$$

$$\lambda_x \frac{\partial \theta}{\partial x} n_x + \lambda_y \frac{\partial \theta}{\partial y} n_y = q, \text{ unitary thermal flux imposed on the surface } S_2;$$

$$\lambda_x \frac{\partial \theta}{\partial x} n_x + \lambda_y \frac{\partial \theta}{\partial y} n_y + \alpha(\theta - \theta_e) = 0, \text{ heat exchange by convection on the surface } S_3.$$

In Equation (1):

1. θ—temperature;
2. λ_x, λ_y—thermal conductivity coefficients of the material from which the body is made;
3. M—unit thermal flow of internal heat sources;
4. q—unit thermal flow through the separation surface S_2;
5. α—the coefficient of heat exchange by convection between the surface S_2 and the surrounding environment;
6. θ_e—the temperature of the surrounding environment.
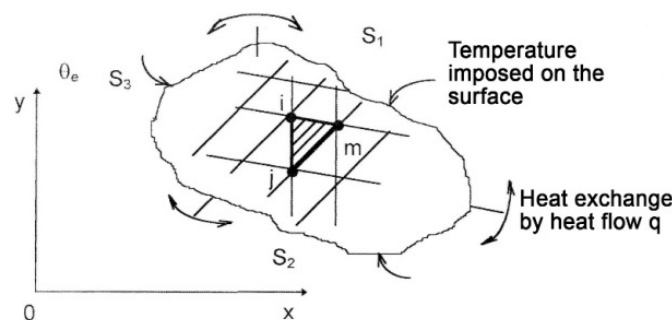
Figure 2. General case of the two-dimensional heat exchange of a body with the surrounding environment, where S_1, S_2, S_3 are surfaces; I,j,m are versors; and θ_e is the temperature of the surrounding environment.

According to the theories of the calculus of variations, solving the differential Equation (1) is equivalent to the minimization of a functional quantity, to the determination of the values of the parameters θ, respectively, for which the functional quantity takes a minimum value. The appropriate function in this case is

$$J = \int_v \left[\frac{1}{2} \left(\lambda_x \left(\frac{\partial \theta}{\partial x} \right)^2 + \lambda_y \left(\frac{\partial \theta}{\partial y} \right)^2 \right) - M\theta \right] dV + \int_{S_3} \alpha\theta \left(\frac{1}{2}\theta - \theta_e \right) dS - \int_{S_2} q\theta dS \quad (2)$$

The first term of the functional corresponds to the heat exchange by conduction. In the differential element $dV_v = dx\,dz\,dz$, $\int_0^h dz = h$ is the constant thickness of the body, which is usually taken as equal to 1. The second term corresponds to the heat exchange by convection through the S_3 surface, and the third term corresponds to the heat exchange by the imposed thermal flux through the S_2 surface.

The minimization of functional 1 is performed on finite elements, the overall effect being obtained by cumulating the partial effects corresponding to each finite element in part. Of the many types of finite elements used today, the triangular ones have the advantage of simplicity.

The temperature variation on the surface of the finite element is described by the shape or interpolation functions, which are characteristic of each type of finite element. These functions express the temperature on the element relative to the temperatures in the nodes. For the triangular finite element (Figure 2):

$$\theta = \begin{bmatrix} N_i\ N_j\ N_m \end{bmatrix} \begin{pmatrix} \theta_i \\ \theta_j \\ \theta_m \end{pmatrix} \quad (3)$$

in which the shape functions are linear relationships of the type:

$$\begin{aligned} N_i &= \frac{(a_i + b_i x + c_i y)}{2\Delta} \\ N_j &= \frac{(a_j + b_j x + c_j y)}{2\Delta} \\ N_m &= \frac{(a_m + b_m x + c_m y)}{2\Delta} \end{aligned} \quad (4)$$

Coefficients a, b, c, are constant quantities, in the expression of which only the coordinates of the nodes of the finite element enter:

$$\begin{array}{lll} a_i = x_j y_m - x_m y_j & a_j = x_m y_i - x_i y_m & a_m = x_i y_j - x_j y_i \\ b_i = y_i - y_m & b_j = y_m - y_i & b_m = y_i - y_j \\ c_i = x_m - x_j & c_j = x_i - x_m & c_m = x_j - x_i \end{array}$$

Minimizing the functional 1 means canceling the derivative of the functional in relation to the parameter θ, that is

$$\frac{\partial J}{\partial \theta} = \begin{pmatrix} \frac{\partial J}{\partial \theta_i} \\ \frac{\partial J}{\partial \theta_j} \\ \frac{\partial J}{\partial \theta_m} \end{pmatrix} = or\ \frac{\partial J}{\partial \theta_i} = \frac{\partial J}{\partial \theta_j} = \frac{\partial J}{\partial \theta_m} = 0 \quad (5)$$

In the following, it is shown how the structural thermal balance equation was established starting from this condition.

Deriving 1 with respect to θ_i and equating to zero, we obtain

$$\frac{\partial J}{\partial \theta_j} \iint \left\{ \lambda_x \frac{\partial \theta}{\partial x} \frac{\partial}{\partial \theta_i} \left(\frac{\partial \theta}{\partial x} \right) + \lambda_y \frac{\partial \theta}{\partial y} \frac{\partial}{\partial \theta_i} \left(\frac{\partial \theta}{\partial y} \right) - M \frac{\partial \theta}{\partial \theta_i} \right\} h\,dx\,dy + \int_{S_3} \left(\alpha\theta \frac{\partial \theta}{\partial \theta_i} - \alpha\theta_e \frac{\partial \theta}{\partial \theta_i} \right) dS - \int_{S_2} q \frac{\partial \theta}{\partial \theta_i} dS = 0 \quad (6)$$

From 2 and 3, it follows that

$$\frac{\partial \theta}{\partial x} = \frac{1}{2\Delta} \left[b_i b_j b_m \right] \begin{pmatrix} \theta_i \\ \theta_j \\ \theta_m \end{pmatrix}$$

$$\frac{\partial \theta}{\partial z} = \frac{1}{2\Delta} \left[c_i c_j c_m \right] \begin{pmatrix} \theta_i \\ \theta_j \\ \theta_m \end{pmatrix}$$

$$\frac{\partial}{\partial \theta_i} \left(\frac{\partial \theta}{\partial x} \right) = \frac{b_i}{2\Delta}, \quad \frac{\partial}{\partial \theta_i} \left(\frac{\partial \theta}{\partial z} \right) = \frac{c_i}{2\Delta},$$

$$\frac{\partial \theta}{\partial \theta_i} = N_i = \frac{1}{2\Delta} (a_i + b_i x + c_i y)$$

substituting in 5, we obtain

$$\frac{h}{4\Delta^2} \iint \left\{ \lambda_x b_i \left[b_i b_j b_m \right] \begin{pmatrix} \theta_i \\ \theta_j \\ \theta_m \end{pmatrix} + \lambda_y c_i \left[c_i c_j c_m \right] \begin{pmatrix} \theta_i \\ \theta_j \\ \theta_m \end{pmatrix} \right\} dx dy + \alpha \int_{S_3} N_i \left[N_i N_j N_m \right] \begin{pmatrix} \theta_i \\ \theta_j \\ \theta_m \end{pmatrix} dS = h \iint M N_i dx dy + \theta_e \alpha \int_{S_2} N_i dS + q \int_{S_2} N_i dS \quad (7)$$

It was assumed that on the sides of the element that exchange heat by convection, α = constant and θ_e = constant, and on the sides on which heat is exchanged by imposed flow, q = constant.

Next, the terms of the two members of Equation (7) will be examined successively.

Left member. Term 1 represents the matrix of thermal conductivity coefficients. Assuming that the limits of a finite element λ_x and λ_z are constant and taking into account that $\iint dx dz = \Delta$, the first term is written in the form:

$$\frac{h}{4\Delta} \left[(\lambda_x b_i b_i + \lambda_z c_i c_i)(\lambda_x b_i b_j + \lambda_z c_i c_j)(\lambda_x b_i b_m + \lambda_z c_i c_m) \right] \begin{pmatrix} \theta_i \\ \theta_j \\ \theta_m \end{pmatrix}$$

Term 2 represents the contribution due to the heat exchange through convection.

$$\alpha \int_{S_3} N_i N_i N_i N_j N_i N_m \right] \begin{pmatrix} \theta_i \\ \theta_j \\ \theta_m \end{pmatrix} dS$$

$$\alpha \int_{S_3} N_i N_j dS = \frac{\alpha}{4\Delta^2} \int_{S_e} (a_i + b_i x + c_i y)(a_j + b_j x + c_j) dS =$$

$$\frac{\alpha}{4\Delta^2} \left\{ \int_{S_3} a_i a_j dS + \int_{S_3} (a_i b_j + a_j b_i) x dS + \int_{S_3} (a_i c_j + a_j c_i) y dS + \int_{S_3} (b_i c_j + b_j c_i) xy dS + \int_{S_3} b_i b_j x^2 dS + \int_{S_3} c_i c_j y^2 dS \right\} =$$

$$\frac{\alpha}{4\Delta^2} \left\{ a_i a_j \int_{S_3} dS + (a_i b_j + a_j b_i) \int_{S_3} x dS + (a_i c_j + a_j c_i) \int_{S_3} y dS + (b_i c_j + c_i b_j) \int_{S_3} xy dS + b_i b_j \int_{S_3} x^2 dS + c_i c_j \int_{S_3} y^2 S \right\} =$$

$$\frac{\alpha}{4\Delta^2} \left[a_i a_j I_0 + (a_i b_j + a_j b_i) I_1 + (a_i c_j + a_j c_i) I_2 + (b_i c_j + b_j c_i) I_3 + b_i b_j I_4 + c_i c_j I_5 \right] = \frac{\alpha}{4\Delta^2} d_i d_j.$$

In this expression, the integrals $I_0 \ldots I_5$ have the following values:

$$I_0 = \int_{S_3} dS = h L_{kl}$$

$$I_1 = \int_{S_3} x dS = \frac{1}{2} h L_{kl} (x_k + x_l)$$

$$I_2 = \int_{S_3} y\, dS = \frac{1}{2} hL_{kl}(y_k + y_l)$$

$$I_3 = \int_{S_3} xy\, dS = \frac{1}{6} hL_{kl}(x_k y_l + x_l y_k + 2x_k y_k + 2x_l y_l)$$

$$I_4 = \int_{S_3} x^2\, dS = \frac{1}{3} hL_{kl}\left(x_k^2 + x_l^2 + x_k x_l\right)$$

$$I_5 = \int_{S_3} y^2\, dS = \frac{1}{3} hL_{kl}\left(y_k^2 + y_l^2 + y_k y_l\right)$$

where:

$L_{kl} = \sqrt{(x_k - x_l)^2 + (y_k - Y_l)^2}$ is the length of the side that exchanges heat through convection, and h is the thickness of the body (Figure 3).
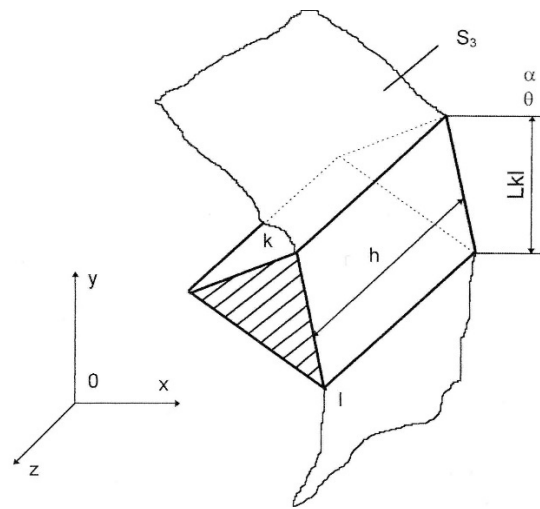
Figure 3. Triangular finite element with constant thickness h in the z-axis direction, having heat exchange by convection through the surface $h \times L_{kl}$, where L_{kl} is the thickness on the y-axis direction, k and l are the dimensions in the section of the triangulated finite element.

The left member of Equation (7) is the first line of the matrix $[k]_e$ of the element.

The other lines are obtained analogously by making $\frac{\partial J}{\partial \theta_j} = 0$ and $\frac{\partial J}{\partial \theta_m} = 0$, so that in the end the left member becomes

$$\frac{1}{4\Delta} \begin{bmatrix} h(\lambda_x b_i b_i + \lambda_y c_i c_i) + \frac{\alpha}{\Delta} d_i d_i & h(\lambda_x b_i b_j + \lambda_y c_i c_j) + \frac{\alpha}{\Delta} d_i d_j & h(\lambda_x b_i b_m + \lambda_y c_i c_m) + \frac{\alpha}{\Delta} d_i d_m \\ h(\lambda_x b_j b_i + \lambda_y c_j c_i) + \frac{\alpha}{\Delta} d_j d_i & h(\lambda_x b_j b_j + \lambda_y c_j c_j) + \frac{\alpha}{\Delta} d_j d_j & h(\lambda_x b_j b_m + \lambda_y c_j c_m) + \frac{\alpha}{\Delta} d_j d_m \\ h(\lambda_x b_m b_i + \lambda_y c_i c_i) + \frac{\alpha}{\Delta} d_m d_i & h(\lambda_x b_m b_i + \lambda_y c_m c_i) + \frac{\alpha}{\Delta} d_m d_i & h(\lambda_x b_m b_m + \lambda_y c_m c_m) + \frac{\alpha}{\Delta} d_m d_m \end{bmatrix}$$

$$\begin{pmatrix} \theta_i \\ \theta_j \\ \theta_m \end{pmatrix} = [k]_e \{\theta\}_e$$

The right member. Term 1 represents the heat flux of the internal heat sources:

$$h \iint MN_i\, dx\, dy$$

Assuming that on the surface of a finite element M = const., and evaluating the shape function in the center of gravity of the coordinate element $\bar{x}$ *and* $\bar{y}$, i.e., expressing the shape function as $N_i = a_i + b_i\bar{x} + c_i\bar{y}$, a sufficiently accurate value is obtained in the form:

$$\frac{M\Delta h}{3}\begin{pmatrix}1\\1\\1\end{pmatrix}$$

which expresses the equal distribution of the flow M on the three nodes of the element. If, instead of the unitary thermal flow of the internal sources, the flow distributed on nodes M_1, M_2, M_3 is known, then

$$M = N_1 M_1 + N_2 M_2 + N_3 M_3$$

so that the first term of the right member is written in the form:

$$h\iint(N_1 M_1 + N_2 M_2 + N_3 M_3)dxdy = \frac{\Delta h}{12}\begin{pmatrix}2M_1 & M_2 & M_3\\M_1 & 2M_2 & M_3\\M_1 & M_2 & 2M_3\end{pmatrix}$$

Term 2 represents the convective exchange through the lateral surface:

$$\theta_e\alpha\int_{S\_3}N_i dS = \theta_e\alpha\int_{S_3}\frac{1}{2\Delta}(a_i + b_i x + c_i y)dS =$$

$$\frac{\alpha\theta_e}{2\Delta}a_i\int_{S_3}dS + \frac{\alpha\theta_e}{2\Delta}b_i\int_{S_3}xdS + \frac{\alpha\theta_e}{2\Delta}c_i\int_{S_3}ydS =$$

$$\frac{\alpha\theta_e}{2\Delta}(a_i I_0 + b_i I_1 + c_i I_2)$$

Term 3 represents the heat exchange through the imposed heat flux:

$$q\int_{S_3}N_i dS = \frac{q}{2\Delta}\int_{S_3}(a_i + b_i x + c_i y)dS = \frac{q}{2\Delta}(a_i I_0 + b_i I_1 + c_i I_2)$$

Overall, for the entire element, the second member of Equation (7) is a column vector of the form:

$$\begin{pmatrix}\frac{M\Delta h}{3} + \frac{\alpha\theta_e + q}{2\Delta}(a_i I_0 + b_i I_1 + c_i I_2)\\\frac{M\Delta h}{3} + \frac{\alpha\theta_e + q}{2\Delta}(a_j I_0 + b_j I_1 + c_j I_2)\\\frac{M\Delta h}{3} + \frac{\alpha\theta_e + q}{2\Delta}(a_m I_0 + b_m I_1 + c_m I_2)\end{pmatrix} = \{F\}$$

Equating the left member with the right one, respectively (*a*) with (*b*), we obtain the thermal balance equation for a finite element:

$$[k]_e\{\theta\}_e = \{F\}_e \tag{8}$$

Summing for all *m* finite elements, the thermal balance equation for the entire section (body) is obtained:

$$\left(\sum_1^m [k]_e\right)\{\theta\} = \{F\}$$

or

$$[K]\{\theta\} = \{F\} \tag{9}$$

where $[K]$ is the thermal conductivity matrix, $\{\theta\}$ is the column-vector of the nodal temperatures, and $\{F\}$ the column-vector of the internal and external thermal fluxes in all nodes of the section. Solving the system of Equation (9) leads to the determination of the temperature in all nodes of the section.

3.2. Axisymmetric Problems

In the case of these problems, which include bodies with axial geometric and thermal symmetry, the functional to be minimized is

$$J = \int_V \left[\frac{1}{2} \left\{ r\lambda_x \left(\frac{\partial \theta}{\partial x} \right)^2 + r\lambda_y \left(\frac{\partial \theta}{\partial y} \right)^2 \right\} - M\theta \right] dV + \int_{S_2} \alpha\theta \left(\frac{1}{2}\theta - \theta_e \right) dS - \int_{S_2} q\theta dS \quad (10)$$

The finite element is a torus with a triangular cross-section (Figure 4).
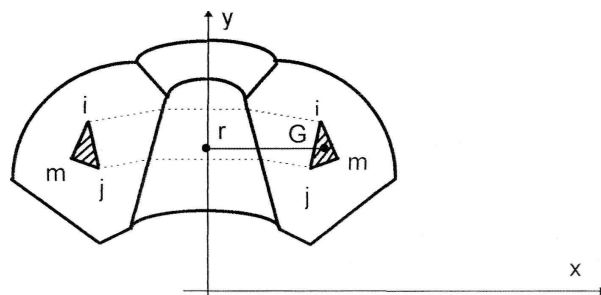
Figure 4. Symmetric body and toroidal finite element with triangular section, where *r* is the radius to the center of gravity *G*.

In the expression of the functional, the radius r appears variable on the surface of the finite element. Sufficiently accurate results are obtained using the radius at the center of gravity, $\bar{r}$. As the differential element is $dV = 2\pi\bar{r}dA$, from $\int_V \bar{r}dV$ we can obtain $2\pi\bar{r}^2 \iint dxdy$.

More accurate results are obtained by using, instead of *r*, the expression *R*, given by

$$R = \frac{1}{12} [r_i r_j r_m] \begin{bmatrix} 2 & 1 & 1 \\ 1 & 2 & 1 \\ 1 & 1 & 2 \end{bmatrix} \begin{Bmatrix} r_i \\ r_j \\ r_m \end{Bmatrix}$$

If the phenomenon of thermal radiation is also taken into account, the general form of the equation of the thermal balance in steady state becomes

$$[K]\{u\} + [R]\{u + Tabs\}4 = \{P\} + \{N\} \quad (11)$$

where:

1. *K*—thermal conductivity matrix;
2. *R*—matrix of heat exchange by radiation;
3. $\{u\}$—vector of unknown temperatures;
4. *Tabs*—the absolute output data of the temperatures required for the calculations of heat exchange by radiation;
5. $\{P\}$—the vector of the applied constant heat flow;
6. $\{N\}$—the vector of temperatures dependent on the heat flows.

The equation is non-linear due to the presence of four terms of the power distribution law developed by radiation.

In addition, nonlinearities due to matrix coefficients and boundary conditions may appear.

These nonlinearities are introduced by specifying material properties and temperature-dependent boundary conditions.

The NASTRAN software applies the Newton–Raphson iteration scheme to solve these nonlinear equations.

The procedure leads to the following form of the thermal balance equation:

$$[KT]_i \{Du\}_i = \{R\}_i \quad (12)$$

where:

1. KT_i—tangential conductivity matrix dz/du;
2. $KT_i = [K]I + 4[R]_i\{ui + Tabs\}3 - \{dN/du\}I$;
3. $\{R\}_i$—the residual vector;
4. $\{R\}_i = \{P\}I + \{N\}i - [K]\{u\} - [R]i\{ui + Tabs\}4$.

At each iteration, the matrix in the left member and the vector in the right member are calculated on the basis of the temperature vector, solving for the unknown vector the new temperature values:

$$\{du\}i = \{ui + 1 - ui\} \tag{13}$$

The program aims to achieve convergence solutions in the optimal sense, balancing various aspects of the solutions, including loading, prior residual data, prior tangent matrix data, etc.

4. Materials and Methods

From a constructive and functional point of view, the MFS seals by means of a class IV tribological coupling (coupling with plane surfaces) [10].

The analyzed MFSs used in this paper are manufactured by ROSEAL S.A., namely EFS 103-S and EF 19 × 45.4 × 3.3. They are used in water pumps and are presented in Figure 5.
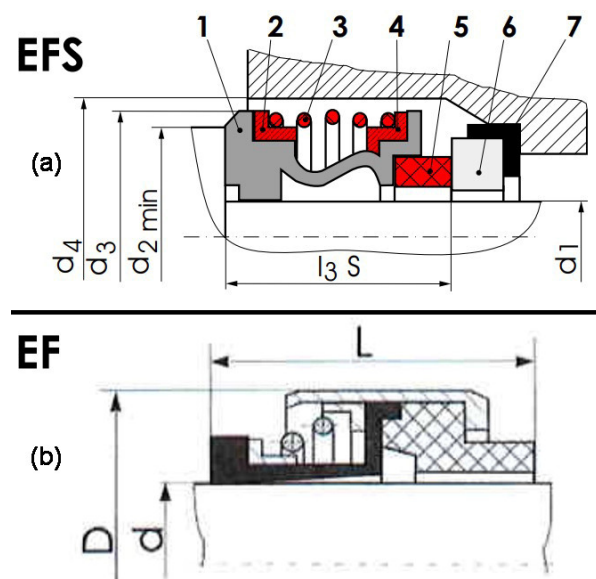
Figure 5. (a) EFS-103-S face seal design: 1. Rubber sleeve; 2. Pressure ring; 3. Spring; 4. Pressure ring; 5. Floating ring; 6. Stationary ring; 7. Rubber gasket. **(b)** EF 19 × 45.4 × 3.3 section and dimensions [32].

The dimensions of MFS EFS-102-S used in the thermodynamical FEM analysis are presented in Table 3.

Table 3. EFS 102-S and EF 19 × 45.4 × 3.3 dimensions as seen in Figure 5 [32].

Nom. Ø	d_1	d_{2min}	d_3	d_4	l_3S	D	d	L
020	20	33	37	38	21.5	39	19	13.3

The stationary ring commonly known as the stationary seat (6) (Figure 5) is immobilized in relation to the housing and constitutes the friction element.

The floating ring (5), in pressed frontal contact with the seat because of the load applied by the spring (3), has the role of a pressure element and rotates together with the shaft.

For reasons of constructive proximity, the sealing function in this case is distributed on two levels. The first level is the primary sealing ensured by pressed and direct contact between the two rings with relative motion. The second level is the secondary sealing, represented by the rubber sleeve to the shaft (1) and to the rubber gasket to the housing (7); they prohibit leaks on the areas of immobile contact with the conjugate parts (bearing cover and shaft).

It is noticed that, in this way, the solution can achieve very high performances conveniently influencing each area.

There are a number of factors that lead to the wear and stress of a front seal, such as contact corrosion, overload, thermal overload, and wear.

Temperature. It appears in the interface of the primary seal due to the heat produced by friction.

Higher temperatures can cause severe wear, gasification of the lubricant film which results in a rapid increase in the coefficient of friction and wear, in some cases exceeding the sintering temperatures of materials, which has the effect of breaking, reciprocal welding or thermal cracking of the rings.

Thermal deformations. The temperature in the interface and its gradients also influence the geometry of the interface [11].

In the case of elastic deformations, the size of the modulus of elasticity of the couple of materials used and the dimensions of the rings are determining factors. The quantifying values of the thermal properties of the materials, i.e., the thermal conductivity (λ), thermal expansion coefficient (α), and heat transfer coefficient (k), combined with the construction of the rings, in turn, influence the temperature gradient and, therefore, the shape of the gap.

Deformation of sealing surfaces. The effects of hydrostatic pressures and temperature differences cause deformations of the rings and of the sealing surfaces, respectively [30].

The thermal effect is very important in the assessment of the total conicity of the gap because the increase in speed causes the increase in power $\left(P_{fr} = \mu r_m \omega F_{ax} \right)$ which, in turn, determines the increase in conicity caused by the uneven heating of the interface.

Two of the factors that influence the level of friction of an annular coupler can be easily highlighted: the couple of materials in contact, namely, the friction rate (μ) and the geometry of the interface.

In conclusion, the stable operation of an MFS can be modified when the thermal and mechanical distortions that can occur are combined with the angular misalignment.

The materials of the primary seal rings used by manufacturers and their physical, mechanical and thermal properties are presented in Table 4 [8,32].

Table 4. Physical-mechanical and thermal characteristics of the materials [8,32].

Characteristics	Tensile Strength	Elastic Modulus	Poisson's Ratio	Hardness	Volumetric Mass	Expansion Coefficient	Thermal Conductivity
Unit	[MPa]	[MPa]	-	H	g/cm^3	10^6 α/°C	W/m °C
G10	540.00	200,000	0.28	135–185 **	7.98	16.00	18.60
U2	125	480,000	0.25	2500 ↖	3.10	50.00	100.00
Y2	41	350–1000	0.50	55–63 ▲	21.00–23.00	70.00	0.233
B1	22.00	50,000	-	29 **	1.65	15/20	2/5

** Brinell hardness; ↖ Knoop hardness; ▲ Shore D Hardness.

The materials are coded [32] as follows:

- G10—stainless steel AISI 316;
- U2—silicon carbide (SiC);
- Y2—polytetrafluoroethylene PTFE + 25% graphite powder;
- B1—carbon graphitic material bonded with resin.

The modeling of frictional contact between the sealing components takes into account the relative movement that occurs between them during operation (n = 3000 rot/min).

The fluid to be sealed is water at a temperature of 80 °C under a pressure of 0.1 MPa.

The corresponding friction rates accepted in the modeling are those evaluated following the measurement of the roughness of the active surfaces of the friction ring coupling [7].

The thermodynamical simulations were made on the two models of MFS earlier mentioned. They were modeled in CAD and imported into the finite element software MSC Nastran.

FEM is a numerical method that can be used to find the solutions to a wide range of engineering problems such as stress analysis, heat transfer analysis, electromagnetic field analysis, or fluid flow analysis.

The method is based on the idea of constructing complicated objects from simpler objects, or the division of complicated objects into simpler objects, called finite elements [FE], for which known calculation schemes can be applied. The operation of dividing the real model into parts of small dimensions is called meshing [33].

In our study we focused on the thermodynamical phenomenon that occurs between the two main elements of the MFS.

The operating temperature of FE with boundary friction in case of natural cooling results from the thermal balance equation [34]:

$$P_{fr} = \mu F_{ax} v = k A_T \Delta t$$
$$t_f = t_0 + \frac{P_{fr}}{k A_T} \leq t_{max}$$

$$(14)$$

where:

k—heat transfer coefficient;

A_T—the free surface (heat exchanger) of the primary seal.

Friction regime and thermal equilibrium are interdependent processes [34]. As a result, the effective rate of friction (μ) and the regime temperature of the friction ring coupling (t_f) are determined iteratively depending on the variation of the lubricants viscosity (v) with temperature (Δt) [9].

In conclusion, the stable operation of a frontal seal can be modified when the thermal and mechanical distortions that can occur are combined with angular misalignment.

The model of the frontal seal made with axially symmetrical finite elements.

From a geometrical point of view, the rings of the primary seal of the MFS have axial symmetry, being composed of rotating bodies (Figure 6). This symmetry means that the modeling problem can be reduced to the modeling of the half section of the seal.
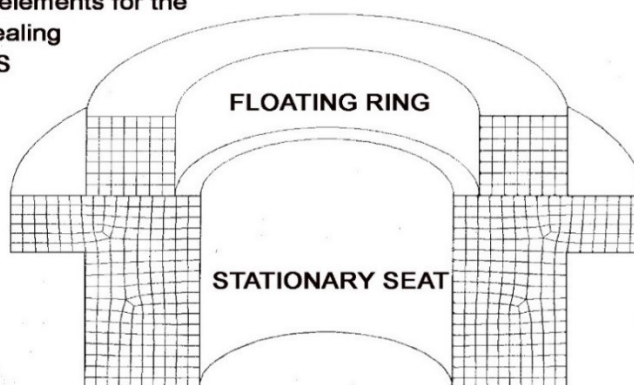
Figure 6. Finite element discretization [31].

The models analyzed with FEM correspond dimensionally and constructively to the component parts of the frontal seals (Figure 5).

The results of the analyses are illustrated in Figure 7a (EFS 103-S) and Figure 7b (EF 19 × 45.4 × 13.3) where we can see the meshed parts.
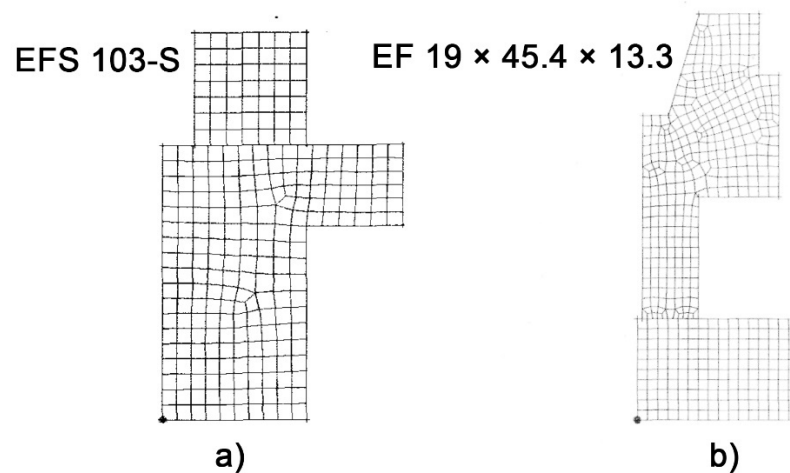
Figure 7. FEM final simplified models use in the simulation.

The analysis of the model is repeated for pairs of materials from the 4 materials presented in Table 4 and coded by the manufacturer.

The contact between the floating and stationary rings is described by a new "slide line" element type that includes the stiffness/friction data, the scale factor and the friction coefficient between the contacting surfaces. The geometric definition of the surfaces in contact includes a series of nodes called "master" and "slave" which belong to the finite sliding surfaces of the deformable bodies and which were defined together with the model discretization.

The "slide line" element is the interaction element between the bodies in contact; its representation in the analyzed model appears as the connecting line between the "master" and "slave" nodes. The coordinate system attached to the "slide line" element is defined by the local coordinate systems of the "master" and "slave" nodes. Each contact zone in the joint assembly is defined by a slide line element.

5. Results

Simulation results. The modeling reproduces the operating behavior of the MFS, respective to EFS 130-S and EF 19 × 45.4 × 13.3. Axial pressure applied to the floating ring will induce a contact pressure field in the interface of the friction ring coupling of the seals. Additionally, this determines the state of tension and the displacements that occur in the front sealing ring.

From a thermal point of view, modeling requires knowledge of:

- The thermal characteristics of the ring materials [8];
- The temperature of the fluid to be sealed;
- The temperature resulting from friction in the interface.

The map of the temperatures and the heat flow in the primary sealing rings for the two types of MFS and for different pair of materials from the FEM analysis are illustrated in Figures 8–11.
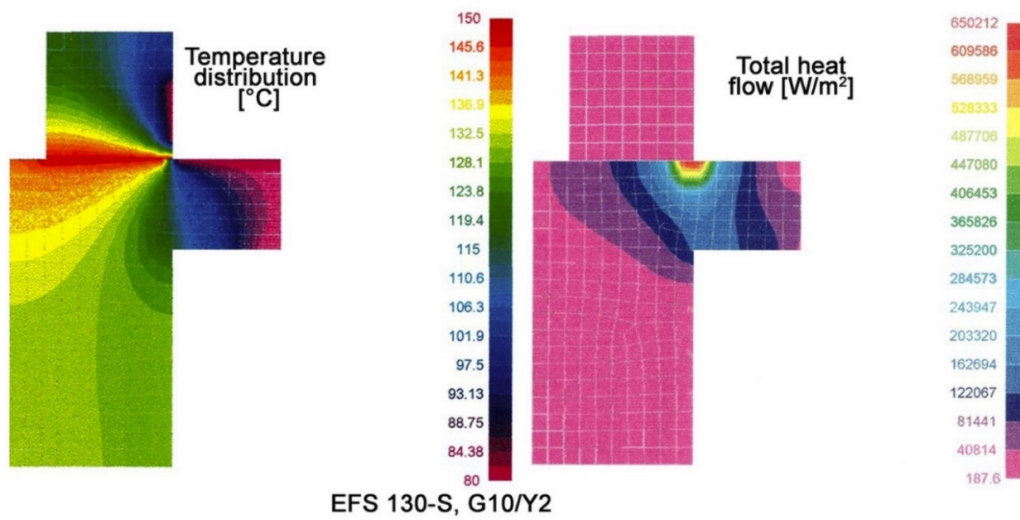
Figure 8. Temperature distribution and total heat flow for MFS, EFS 103−S, G10/Y2.
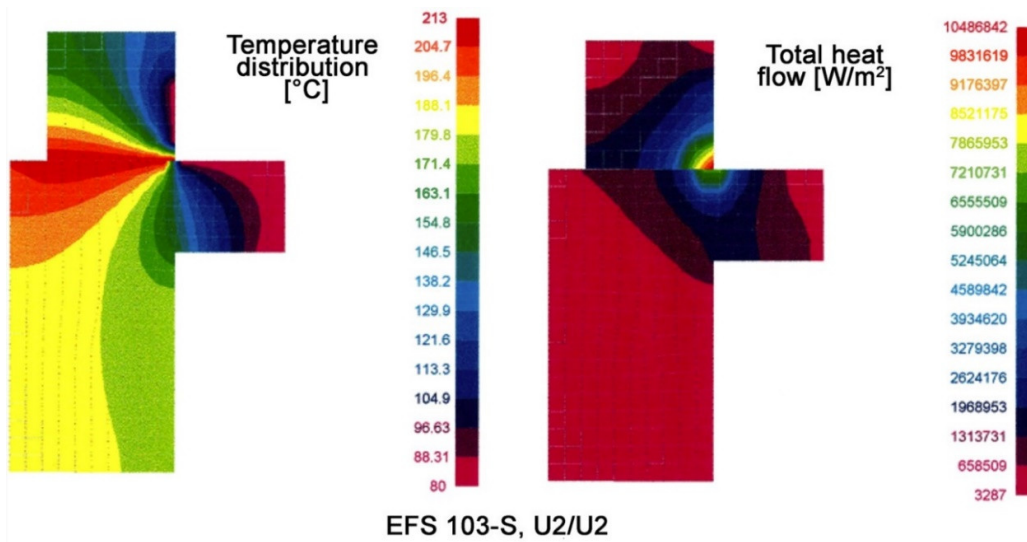
Figure 9. Temperature distribution and total heat flow for MFS, EFS 103−S, U2/U2.
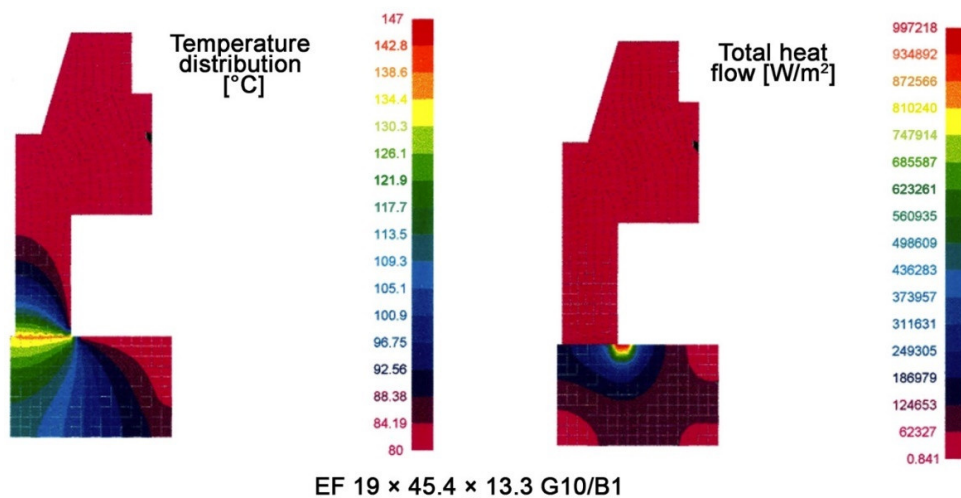
Figure 10. Temperature distribution and total heat flow for MFS, EF 19 × 45, G10/B1.
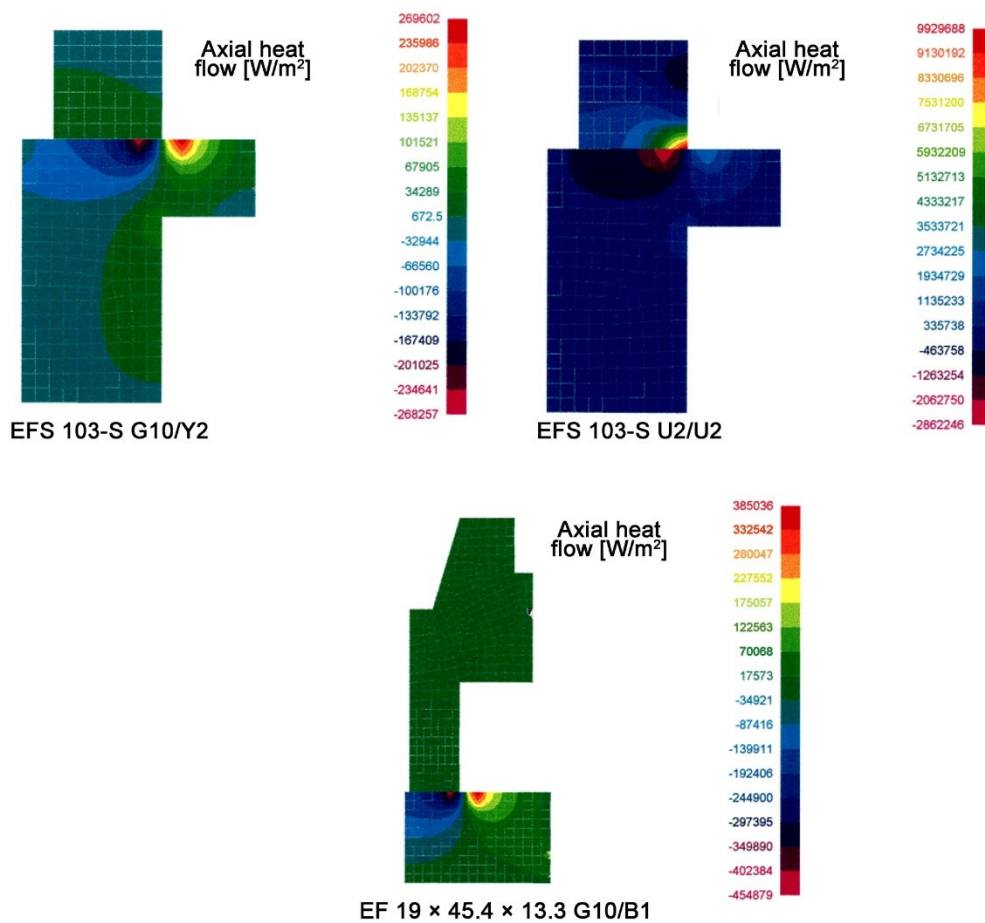
Figure 11. Axial heat flow results for MFS, EFS 103−S, G10/Y2, U2/U2 and MFS, EF 19 × 45, G10/B1.

After the postprocessing, the distributions of temperatures and the thermal loading along the interface of the primary sealing are also obtained (Figures 12–14).
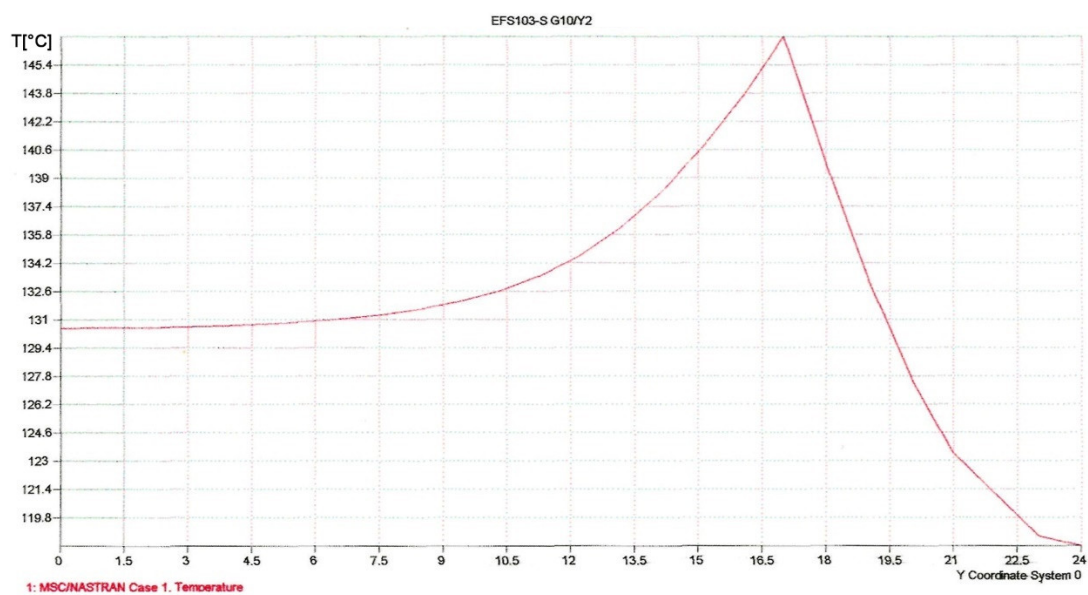
Figure 12. Thermal loading of the rings for EFS 103−S, G10/Y2, along the interface.
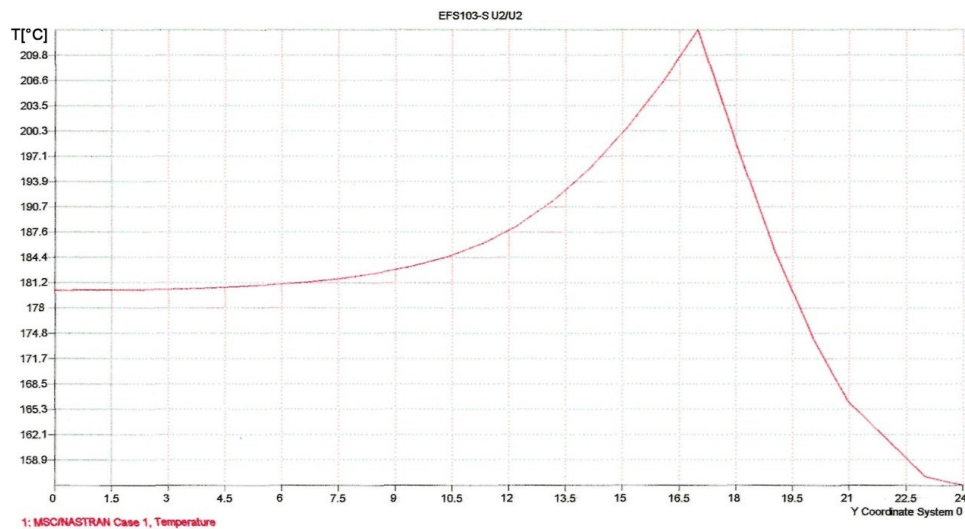
Figure 13. Thermal loading of the rings for EFS 103−S, U2/U2, along the interface.
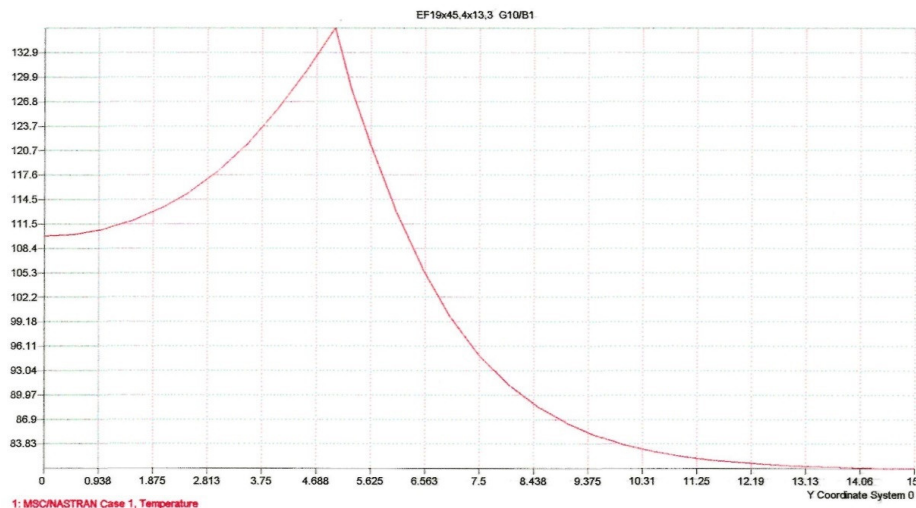
Figure 14. Thermal loading of the rings for EF19 × 45,4 × 13,3, G10/B1, along the interface.

Based on the parameters determined by FEM analysis, the leakage rates can be evaluated. In the case of the non-isothermal flow of an incompressible fluid for an axial-symmetrical configuration [35,36], the Reynolds equation is

$$\frac{d}{d_r}\left(\frac{h^3}{\eta}\frac{d_p}{d_r}\right) = 0 \tag{15}$$

where:

$r = d/2$;

h—the dynamic viscosity of the working fluid.

Considering that at the limit, in the mentioned case, the interface leakage flow rate is given by the relation:

$$Q = \frac{\pi d_m \Delta p h^3}{12 \eta b} \tag{16}$$

where:

$d_m = 0.5(d + D)$;

$b = 0.5(D - d)$;

$h = 0.5(R_{z1} + R_{z2})$;

Δp—the pressure drop in the interface;

$R_{z1/2}$—the contact roughness;

The dynamic viscosity varies depending on the temperature (T) of the fluid according to a polynomial dependence:

$$\eta = \frac{\eta_f}{1 + (T - T_F)} \qquad (17)$$

where:

η_f = the dynamic viscosity at reference temperature.

The power dissipated through friction in the interface is

$$P_{fr} = \mu p_a A_T r_m \omega \qquad (18)$$

where:

μ—the friction rate in the interface;

$A_T = \pi(D^2 - d^2)/4$

ω—the angular velocity of the floating ring

And it transforms into heat:

$$P_{fr} = k_T A_T \left(T - T_f\right) \qquad (19)$$

where:

$$k_T = \frac{\lambda_1}{l_1} + \frac{\lambda_2}{l_2}$$

$\lambda_{1/2}$—the thermal conductivity of the ring materials;

$l_{1/2}$—the axial dimensions of the rings.

The debit relation becomes

$$Q = \frac{A_T h^3}{12b^2} \frac{\Delta p}{\eta_f} \left(1 + \frac{\mu p_a A_T \omega}{2\pi b k_T}\right) \qquad (20)$$

or

$$Q = \frac{A_T h^3}{12b^2} \frac{\Delta p}{\eta_f} 1 + \frac{\mu}{k_T} (pv) \qquad (21)$$

From relations (20) and (21), we can see the direct dependence between the leakage flow rate Q, the product (*pv*) and the heat transfer coefficient k_T, values that, in turn, characterize the operation of a seal, of a sliding bearing, respective to a heat exchanger.

Customizing relation (20) for the MFS analyzed and taking into account the FEM results, the flow rate-angular velocity dependences are obtained (Figures 15 and 16).
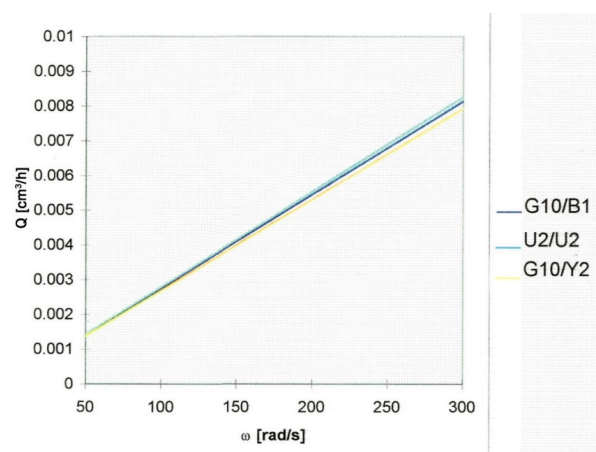
Figure 15. Variation of the leakage loss flow at an EFS103-S front seal as a function of the angular velocity and for different material couplings of the primary seal.
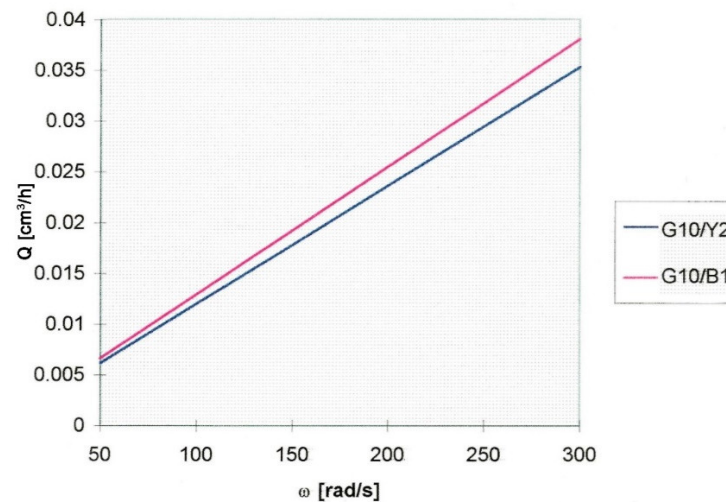
Figure 16. Variation of the leakage loss flow at a frontal seal EF19 × 45.4 × 13.3 depending on the angular speed and for different material couplings of the primary seal.

The results of the analysis highlight the fact that the flow rate of leaks varies linearly with increasing the angular speed of the pressure ring and is independent of the materials used in the primary seal.

The values of leakage losses due to the leakiness of the MFS analyzed are far below the values allowed by Richtlinie VDI 2440, namely 1 cm^3/h (12 g/h) [37].

6. Discussion

From a thermal point of view, the physical-mechanical and thermal properties of the working fluid and the materials of the primary seal of the MFS have a major influence on the operating behavior of the MFS. Thus, the materials of the primary seal must have a low coefficient of friction, to allow a quick evacuation of the heat produced, to have a low coefficient of expansion and not to damage each other.

From the FEM analysis, the results are as follows:

- The maximum temperature is reached in the forecast area of the interface of the primary seal;
- We can determine the limits of the rings' ability to take over a certain power lost through friction without exceeding certain temperatures (targeting the choice of materials);
- With the help of the model, it is possible to quickly and precisely determine the extreme temperatures of the rings;
- The temperature distribution allows the analytical evaluation of the performance of the front seals (see the expression for calculating the loss flow rate);
- The axial distribution of the temperature is not linear as approximated in the literature [36,38,39];
- The temperature gradient in the axial direction is a decisive factor in the thermal deformation of the rings with a direct effect on the geometry of the interface;
- The temperature variation in the radial direction is insignificant;
- There is a large temperature gradient in the axial direction near the interface;
- Taking also into account the phenomenon of convection at the level of the pressure ring/medium, the relatively high values of the heat transfer coefficient k_T resulting from the thermal analysis are observed.

The FEM results also allow the variation of the heat transfer coefficient k_T in the axial direction to be determined and the value of the convection coefficient starting from the power is dissipated.

Until now, the focus has been on electric motor efficiency and this is seen in the trends in energy efficiency technologies widely used around the world (energy efficient motors, energy saving soft starters, variable speed drives, energy efficient transformers, etc.) This

paper presents a new approach by taking a step further looking for energy efficiency methods resulting from extending the life of MFS [40].

7. Conclusions

Increasing the life expectancy of the seals automatically generates lower operating costs, low maintenance costs, low losses from equipment downtime during repair, avoiding the risk of other equipment failures.

A good part of the maintenance activity also includes the replacement of mechanical seals, considered as wear parts. According to the report "Global Mechanical Seals Market Size by Design (Pusher Type Mechanical Seals, Non-Pusher Type Mechanical Seals), By End User Industry (Oil and Gas, Chemical, Mining), By Geographic Scope and Forecast," the mechanical seals market size was valued at EUR 3.64 billion in 2022.

Active control of the MFS will overcome the limitation of reliability, allowing a particularly reliable seal and a priori estimation of wear over time. Increasing the life of MFS offers great economic benefits in the top fields, such as nuclear, aeronautical, chemical, petrochemical, pharmaceutical, food, domestic, and transportation fields.

There are a number of factors that lead to the wear and stress of a front seal, such as contact corrosion, overload, thermal overload, and wear. Temperature appears in the interface of the primary seal due to the heat produced by friction. The temperature in the interface and its gradients also influence the geometry of the interface.

A realistic approach to the MFS phenomenology can only be made through a thermo-hydrodynamic analysis.

From a thermal point of view, the physical-mechanical and thermal properties of the working fluid and the materials of the primary seal of the MFS have a major influence on the operating behavior of the MFS.

In the paper, the thermodynamic FEM analysis was made using the MSCNASTRAN software and was carried out for two types of MFS, namely EFS-103-S and EF 19 × 45.4 × 3.3, with an operation field of n = 3000 rot/min, water at 80 °C, pressure of 0.1 MPa and for various pairs of materials of the primary seal.

The results highlight the following aspects:

- The maximum temperature is reached in the forecast area of the interface of the primary seal;
- The limits of the rings' ability to take over a certain power lost through friction without exceeding certain temperatures (targeting the choice of materials);
- It is possible to quickly and precisely determine the extreme temperatures of the rings;
- The temperature distribution allows the analytical evaluation of the performance of the front seals, namely the loss flow rate;
- The axial distribution of the temperature is not linear as approximated in the literature;
- The temperature gradient in the axial direction is a decisive factor in the thermal deformation of the rings with a direct effect on the geometry of the interface;
- The temperature variation in the radial direction is insignificant; there is a large temperature gradient in the axial direction near the interface;

Additionally, taking into account the phenomenon of convection at the level of the pressure ring/medium, relatively high values of the heat transfer coefficient k_T resulting from the thermal analysis are observed.

The FEM results also allow the determination of the variation of the heat transfer coefficient k_T in the axial direction and the value of the convection coefficient starting from the power dissipated.

The conclusions are that energy saving solutions are available and there is potential to save many labor hours and waiting time caused by maintenance procedures, replace parts, and increase overall efficiency (factors that can all be quantified in energy according to the first law of thermodynamics) by simply choosing better pairs of materials, even if they have an initial higher cost.

Considering the global tendencies in energy demand and availability, researchers recommend using reliable design solutions whenever possible and FEM analysis in the detriment of experimental research because of the possibility of saving time and resources, not only in the case of MFSs, but also in any endeavor.

We recommend that energy efficiency techniques emphasize studying the link between the MFS (focused on increasing the lifetime of the seal) and the energy consumption of electric motors, and how significant savings can be achieved in this sector of energy, taking into account that, in our study, we have a total energy loss of 8 euros/hour (according to Table 1).

References

1. Lai, T.W. Development of High Pressure–Velocity Contacting Plain Face Seals for Sealing Water. *Tribol. Trans.* **2020**, *63*, 477–486. [CrossRef]
2. Hill, R. Mechanical seal alliance agreements. *Seal. Technol.* **2003**, *2003*, 5–8. [CrossRef]
3. Available online: https://www.verifiedmarketresearch.com/product/mechanical-seals-market (accessed on 29 September 2022).
4. Errigo, A.; Choi, J.-K.; Kissock, K. Techno-economic-environmental impacts of industrial energy assessment: Sustainable industrial motor systems of small and medium-sized enterprises. *Sustain. Energy Technol. Assess.* **2022**, *49*, 101694. [CrossRef]
5. Available online: https://www.conurbant.eu/file/2415-PAED_Municipiului_Timisoara_2014-2020_reevaluat_in_2014_publishing_online.pdf (accessed on 29 September 2022).
6. Available online: https://www.pumpsandsystems.com/guide-energy-efficient-sealing-solutions (accessed on 29 September 2022).
7. Argeşanu, V. Asigurarea Funcțional Constructivă a Durabilității Optime Pentru Etanşările Frontale cu Contact Direct. Ph.D. Thesis, Timișoara Polytechnic University, Timișoara, Romania, 1998.
8. Mayer, E. *Mechanical Seals Paperback*; Butterworth-Heinemann: Oxford, UK, 2013.
9. Straffelini, G. *Friction and Wear*; Springer: New York, NY, USA, 2015.
10. Kragelsky, I.V. *Friction Wear Lubrication: Tribology Handbook Paperback*; Pergamon Press: Oxford, UK, 2013.
11. Hetnarski, R.B. *Thermal Stresses—Advanced Theory and Applications*; Springer Nature: New York, NY, USA, 2019.
12. Zheng, W.; Sun, J.; Ma, C.; Yu, Q. The Theoretical Basis of Face Contact Pressure Design of the Zero-Leakage Mechanical Seal. *Coatings* **2022**, *12*, 536. [CrossRef]
13. Bai, S.; Hao, J.; Yang, J.; Song, Y. Gas-Liquid Mass Transfer Behavior of Upstream Pumping Mechanical Face Seals. *Materials* **2022**, *15*, 1482. [CrossRef]
14. Peng, X.D.; Xie, Y.B.; Gu, Y.Q. Evaluation of mechanical face seals operating with hydrocarbon mixtures. *Tribol. Int.* **2003**, *36*, 199–204. [CrossRef]
15. He, W.; Wang, S.; Zhang, C.; Wang, X.; Liu, D. A Wear Simulation Method for Mechanical Face Seals under Friction Instability Conditions. *Appl. Sci.* **2020**, *10*, 2875. [CrossRef]
16. Meseguer, J.; Pérez-Grande, I.; Sanz-Andrés, A. Mechanical Interfaces. In *Spacecraft Thermal Control*; Elsevier: Amsterdam, The Netherlands, 2012; pp. 157–173.
17. Gani, M.; Santos, I.F.; Grann, H. Model validation of mechanical face seals in two-phase flow conditions. *Trybology Int.* **2022**, *167*, 107417. [CrossRef]
18. Blasiak, S. Heat Transfer Analysis for Non-Contacting Mechanical Face Seals Using the Variable-Order Derivative Approach. *Energies* **2021**, *14*, 5512. [CrossRef]
19. Ma, Y.; Wang, Y.H.; Su, W.T. Characteristics of the Waviness End-Face Mechanical Seal in Reactor Coolant Pump Considering the Viscosity-Temperature Effect. *Front. Ebergy Res.* **2021**, *9*, 647. [CrossRef]
20. Feng, X.D.; Su, W.T.; Tan, H.P. Numerical and Experimental Study on Waviness Mechanical Seal of Reactor Coolant Pump. *Processes* **2020**, *8*, 1611. [CrossRef]
21. Dingui, K.; Brunetiere, N.; Adjemout, M. Surface Texturing to Reduce Temperature in Mechanical Seals. *Tribol. Online* **2020**, *15*, 222–229. [CrossRef]
22. Wos, S.; Koszela, W.; Pawlus, P. The effect of graphite surface texturing on the friction reduced in dry contact. *Tribol. Int.* **2020**, *151*, 106535. [CrossRef]

23. Jones, G.A. On the Tribological behaviour of mechanical seal face materials in dry line contact—Part I. Mechanical carbon. *Wear* **2004**, *256*, 415–432. [CrossRef]

24. Song, Y.Z.; Zhai, G.T.; Song, J.R.; Li, G.S.; Shi, J.L.; Guo, Q.G.; Liu, L. Seal and wear properties of graphite from MCMb/pitch-based carbon/phenolic-based carbon composites. *Carbon* **2006**, *44*, 2793–2796. [CrossRef]

25. Xu, L.S.; Wu, J.H.; Yuan, X.Y. Lubrication and stability enhancement by attaching superconducting magnetic force on non-contacting mechanical seals for reusable rocket turbopump. *Proc. Inst. Mech. Eng.—J. Eng. Tribol.* **2022**, *236*, 892–907. [CrossRef]

26. Zhou, X.; Chen, Z.; Wang, J.H. Thermo-mechanical coupling analysis of the end faces for a mechanical seal under dry friction. *Tribol. Int.* **2021**, *160*, 107050. [CrossRef]

27. Cavalcante, J.P.D.; Maciel, D.N.; da Silva, J.N. A Simple FEM Formulation Applied to Nonlinear Problems of Impact with Thermomechanical Coupling. *Lat. Am. J. Solids Struct.* **2017**, *14*, 2439–2462. [CrossRef]

28. Schinder, D.S.; Stephens, L.S. An experimental study on the impact of interface temperature on thermally induced wear transitions in dry sliding. *J. Tribol.—Trans. Asme* **2006**, *128*, 460–468. [CrossRef]

29. Zhao, W.G.; Zhang, G.Y.; Dong, G.N. Friction and wear behavior of different seal materials under water-lubricated conditions. *Friction* **2021**, *9*, 697–709. [CrossRef]

30. Lebeck, A.O. *Principles and Design of Mechanical Face Seals*, 1st ed.; John Wiley & Sons, Inc.: New York, NY, USA, 1991.

31. Argesanu, V.; Mocuţa, G.E. *Modelarea Problemelor Neliniare cu Ajutorul Metodei Elementului Finit*; Editura Mirton Timisoara: Timișoara, Romania, 1999.

32. Roseal.eu. Available online: https://fdocumente.com/document/sc-roseal-sa-etansarile-mecanice-cunoscute-realizind-etansare-durata-de-functionare.html?page=1 (accessed on 15 September 2022).

33. Lakshmi, N.G. *Finite Element Analysis*; BS Publications: Hyderabad, India, 2021.

34. Lewandowski, J.J.; Lowhaphandu, P. Effects of hydrostatic pressure on mechanical behaviour and deformation processing of materials. Taylor & Francis Online. *Int. Mater. Rev.* **1998**, *43*, 145–187.

35. Mohamad, A.A. Isothermal Incompressible Fluid Flow. In *Lattice Boltzmann Method*; Springer: London, UK, 2019. [CrossRef]

36. Baskharone, E.A.; Hensel, S.J. Moment coefficients of incompressible-flow seals with conically whirling rotors. *Int. J. Sci.* **1991**, *33*, 151–167. [CrossRef]

37. Vdi.de. Available online: https://www.vdi.de/richtlinien/details/vdi-2440-emission-control-mineral-oil-refineries (accessed on 5 October 2022).

38. Chapman, A.J. *Fundamentals of Heat Transfer*; McMillan Pubiishing Co.: New York, NY, USA, 1987.

39. Pascovici, M.D. A Termohydrodynamic Analysis of a Misalignes Mechanical Face Seal. *Tribol. Trans.* **1993**, *36*, 589–596.

40. Maheswaran, D.; Rangaraj, V.; Jembu Kailas, K.K.; Adithya Kumar, W. Energy efficiency in electrical systems. In Proceedings of the 2012 IEEE International Conference on Power Electronics, Drives and Energy Systems (PEDES), Bengaluru, India, 16–19 December 2012; IEEE: Toulouse, France, 2012; p. 13400181.